Bridging the Micro and Macro Mechanical Behaviour of Granular Materials

Q Zhao[1*], Y Chen[2], G Ma[3]

[1]The Hong Kong Polytechnic University, Hong Kong, China
[2]Changjiang Survey, Planning, Design and Research Co., Ltd., Wuhan, China
[3]Wuhan University, Wuhan, China

*Corresponding author
doi: https://doi.org/10.21467/proceedings.133.23

ABSTRACT

Understanding the underlying physics and mechanisms responsible for the loss of stability of granular systems is crucial to the mitigation of geohazards such as landslides and earthquakes. We use a combination of in situ testing under X-ray micro-computed tomography (micro-CT) and the hybrid finite and discrete element method (FDEM) to investigate the mechanical behaviours of granular materials from the microscopic to the macroscopic scales. We conduct a miniature triaxial test on a granular column sample that is imaged with X-ray micro-CT at incremental strain steps. Then, spherical harmonic (SH) analysis is performed to characterize and reconstruct the multi-scale morphological characteristics of particles, which was used to create the digital twin of the tested sample. FDEM simulation quantitatively agrees with the overall response observed in the experiment. We find that the granular material deforms plastically through spatially localized zones of large nonaffine displacements, and the spatiotemporal evolution of these zones controls the macroscopic responses of the system. Our method sheds light on bridging length scales from microscopic scale to macroscopic granular systems.

Keywords: In Situ Test Under Micro-CT, Granular Material, Digital Twin

1 Introduction

Mechanical behaviour of granular materials in nature is related to geohazards such as landslides, soil foundation instability, and earthquakes. The granular system responds to the mechanical perturbation through the spatial rearrangement of particles and the dynamics of force transmission network (Majmudar & Behringer, 2005). Therefore, it is crucial to understand the underlying physics and mechanisms responsible for the loss of stability of granular systems.

X-ray micro computed tomography (micro-CT) is a non-destructive approach of examine material internal structures. Micro-CT have been successfully used to characterize the structural properties and microscopic scale dynamics of different materials (e.g., Andò et al., 2012; Weis & Schröter, 2017; Q. Zhao et al., 2018; Q. Zhao et al., 2020). X-ray computed tomography aided laboratory test allows for the investigation of granular materials from microscopic to macroscopic scales (e.g., Karatza et al., 2017; Afshar et al., 2018; Cheng & Wang, 2018; Kong & Fonseca et al., 2019; Chevalier et al., 2019), making it a promising tool in studying the behaviour of complex granular systems. This technology was used to measure contact forces among particles (e.g., Saadatfar et al., 2012; Andrade & Avila, 2012). However, it was only applied to granular systems with small number of particles. Tracking the trajectory of large number of moving particles and evaluating their interactions remains a challenging task, especially for the granular systems that experience large deformation.

The particle based numerical simulation methods provide a different perspective to examine the behaviour of granular systems. Previous studies suggested that particle shape has profound influences on granular dynamic behaviour, which promoted the development of advanced modelling techniques (Alshibli et al., 2016; Murphy et al., 2019), such as the discrete element method (DEM)

Proceedings DOI: 10.21467/proceedings.133; Series: AIJR Proceedings; ISSN: 2582-3922; ISBN: 978-81-957605-1-0

(e.g., Wu et al., 2020), the hybrid finite and discrete element method (FDEM) (Ma et al., 2014; Ma et al., 2016; Chen et al., 2021), and the level set DEM (LS-DEM) method (Kawamoto et al., 2016; Kawamoto et al., 2018).

In this study, we investigate the microscopic and macroscopic behaviour of granular materials by combining in situ testing under X-ray micro-CT and FDEM modelling. With this novel combination of technologies, we achieved a quantitative description of the macroscopic responses and microscopic dynamics of the granular system during the whole deformation process.

2 Material and Methods

2.1 In Situ Testing under X-ray Micro-CT

The experiment was carried out using the in situ testing apparatus under micro-CT (ERDμ) developed by Q. Zhao et al. (2017) (Figure 1). The apparatus consists of a control panel and an X-ray transparent loading vessel (Figure 1a). Data acquisition equipment and drivers of the step motors are mounted on the control panel. During an in situ testing, the whole system is placed inside the cabinet of the micro-CT (Figure 1 b&c). This apparatus can conduct unconfined (uniaxial) compression tests, confined compression tests, and rotary shear tests.

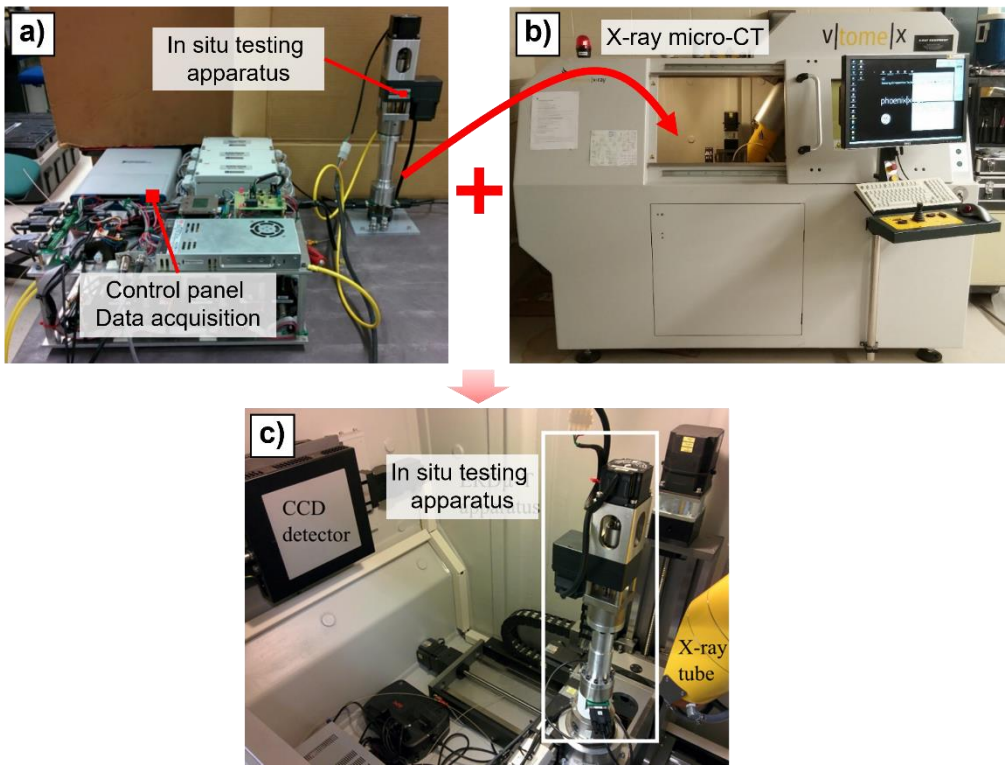

Figure 1. The in-situ testing apparatus under X-ray micro-CT. (a) the control panel and the X-ray transparent loading vessel, (b) the X-ray micro-CT machine, and (c) the testing apparatus seated inside the micro-CT during the test.

2.2 Sample preparation and Testing Procedure

The sample is made of Ottawa sand and has an initial diameter of approximately 12 mm and a height of 25 mm. It is prepared using the dry pluviation method and subjected to vibration and tapping until a dense packing is achieved. The sample is confined by a 0.3 mm thick flexible latex membrane, providing the flexible boundary condition while allowing for the application of confining pressure. Then, the sample is placed inside the ERDμ apparatus that is mounted on the rotation table inside the X-ray micro-CT (Figure 2a). During the experiment, the specimen was first isotropically compressed

Proceedings DOI: 10.21467/proceedings.133
ISBN: 978-81-957605-1-0

Series: AIJR Proceedings
ISSN: 2582-3922

to the confining pressure (σ_3) of 300 kPa and then the axial stress (σ_1) is increased by the downward movement of the top loading platen at a constant strain rate of 0.1%/min (Figure 2b).

Three dimensional (3D) micro-CT scans of the sample were acquired at 15 strain levels. The first scan was conducted after the application of the confining pressure. During each 3D scan, 1080 two dimensional (2D) radiographic projections with a pixel size of 27.5 μm were acquired, while the ERDμ apparatus was rotated 360° around the vertical axis. The loading platen was kept stationary during scans and the confining pressure was maintained constant throughout the experiment. The imaging of the incrementally strained sample allowed us to investigate the gradual variation of the sample internal structures.

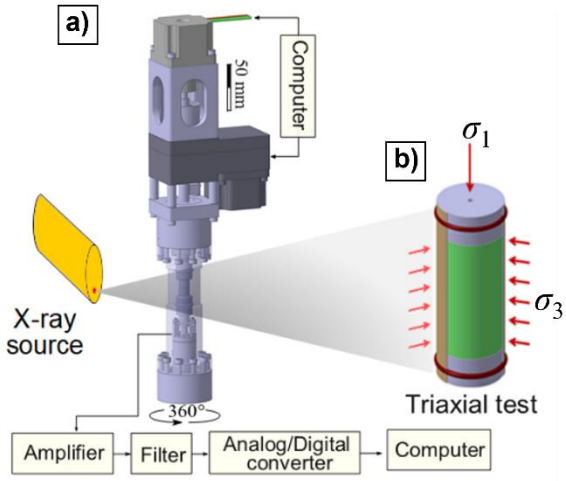

Figure 2: Schematic diagram of the experimental setup. (a) The ERDμ X-ray transparent testing vessel. (b) The sample assembly and loading conditions in the experiment test.

2.3 Image Processing

The 2D radiographic projections were reconstructed into a 3D digital volume of the sample, with the grey values of the voxels directly related to the density of the sample at the corresponding spatial coordinates (Figure 3 a-b). Then, the digital volume was divided into two phases: air and solid, based on global thresholding. In the binarized image, contacting grains are connected due to the partial volume effect, and a mark-controlled watershed segmentation was used to separate the grains. This watershed algorithm uses the image morphology to identify the grains and separate them from each other. Finally, the separated grains are labelled for further tracking and analysis (Figure 3c). Contacts between neighbouring particles can be identified by subtracting the watershed segmented data from the binarized data.

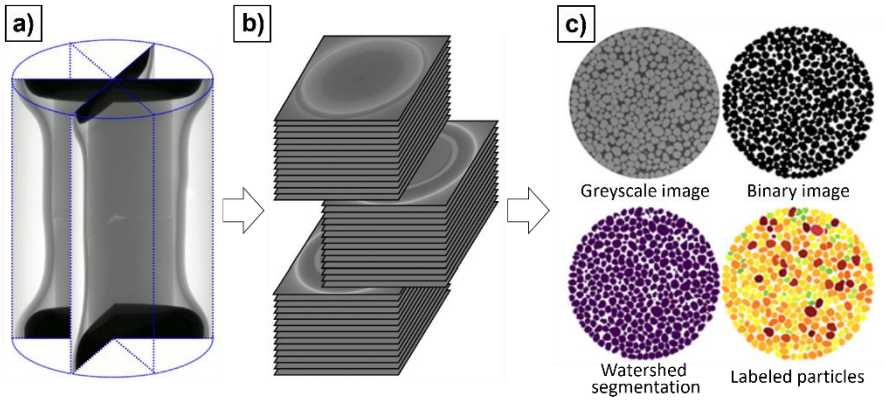

Figure 3: Image processing procedure. (a) Raw radiographic projection images, (b) horizontal image stack after reconstruction, and (c) image thresholding, watershed segmentation, and labelling.

Particle morphological features such as the particle volume, surface area, and principal axis lengths of the particle are used in particle matching and tracking algorithms. These morphological quantities

are sensitive to the X-ray CT imaging quality. One promising approach of improving the matching accuracy is to use more morphological features ranging from particulate size to surface texture. Spherical harmonic (SH) analysis mathematically describes the general conformation of the particle shape at different scales. SH analysis is capable of characterizing and quantifying the multiscale morphological features of irregularly shaped particles (Garboczi, 2002; Zhou et al., 2015; Wei et al., 2018). The SH invariants, independent of particle translation and rotation, are adopted in evaluating the similarities of particles to track particles across multiple loading steps (Kazhdan et al., 2003; B. Zhao et al., 2017; B. Zhao et al, 2018).

We use SH function to represent the surfaces of particles extracted from image data:

$$r(\theta,\varphi)=\sum_{n=0}^{\infty}\sum_{m=-n}^{n}c_n^m Y_n^m(\theta,\varphi) \quad \textbf{(1)}$$

$$Y_n^m(\theta,\varphi)=\sqrt{\frac{(2n+1)(n-m)!}{4\pi(n+m)!}}P_n^m(\cos\theta)e^{im\varphi} \quad \textbf{(2)}$$

where $r(\theta,\varphi)=\sqrt{\sum_{x,y,z}(\kappa-\kappa_0)^2}$ is the polar radius from particle centroid (x_0, y_0, z_0), $\theta\in[0,\pi]$ and $\varphi\in[0,2\pi]$ are the spherical coordinates, and c_n^m is the corresponding SH coefficient. Taking $r(\theta,\varphi)$ as the input on the left side of Eq. (1), a linear equation system with $(n+1)^2$ unknowns can be obtained to determine coefficients c_n^m. $P_n^m(\cos\theta)$ is the Legendre function of degree n and order m, expressed by Rodrigues's formula:

$$P_n^m(x)=(1-x^2)^{|m|/2}\cdot\frac{d^{|m|}}{dx^{|m|}}\left[\frac{1}{2^n n!}\cdot\frac{d^n}{dx^n}(x^2-1)^n\right] \quad \textbf{(3)}$$

We define a set of SH frequencies as $R_n(\theta,\varphi)=\sum_{m=-n}^{n}c_n^m Y_n^m(\theta,\varphi)$, which exhibit rotational invariant properties independent of particle translation and rotation (Kazhdan et al., 2003), and the modulus of the SH frequency, that is, the SH rotation-invariant is calculated as:

$$\left\|R_n(\theta,\varphi)\right\|=\sqrt{\int_0^{2\pi}\int_0^{\pi}R_n(\theta,\varphi)^2\,d\theta d\varphi}=\sqrt{\sum_{m=-n}^{n}\left\|c_n^m\right\|^2} \quad \textbf{(4)}$$

The SH coefficients describe the general conformation of the particle shape at different scales. While a high SH degree can represent the shape of the grains with fine details, it was found that an SH degree of 15 is sufficient to describe the grains in this study. For natural sand, there are no two particulates with completely identical morphological features; therefore, the unique set of SH rotation-invariants can be used as the geometrical DNA for matching particles.

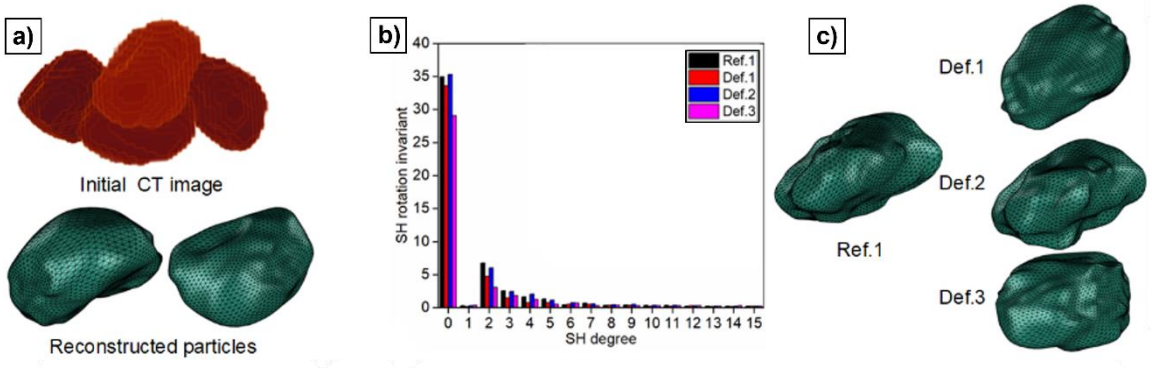

Figure 4: (a) Mathematical characterization of the particles based on spherical harmonic (SH) reconstruction. (b) Statistical difference of the derived spherical harmonic rotation-invariants at different SH-degrees. Comparison is shown between one particle from the Reference configuration (Ref.) and three particles from deformed configuration (Def.). (d) Examples of the digital reconstruction and matching results.

Proceedings DOI: 10.21467/proceedings.133
ISBN: 978-81-957605-1-0

Series: AIJR Proceedings
ISSN: 2582-3922

Lastly, we can identify the matching particles between adjacent loading states by evaluating the minimum $L^2\text{-}norm$ difference between the corresponding vectors $\mathbf{R}_n$ (B. Zhao et al., 2018), measured by

$$\left\| R_n^k(\theta,\varphi) - R_n^{k+1}(\theta,\varphi) \right\| = \sqrt{\sum_{n=0}^{\infty} \left(\left\| R_n^k \right\| - \left\| R_n^{k+1} \right\| \right)^2} \quad (k = 1, 2, \mathrm{K}, N_S) \qquad \textbf{(5)}$$

where k is the loading states and N_S is the total number of micro-CT scans. With this particle characterization and matching method, we successfully tracked the movement of almost all the particles and created a library of the multiscale morphological information of the granular material tested in the experiment (Figure 4).

2.4 Creation of the Digital Twin

We built a digital twin of the laboratory sample using the FDEM method. A typical FDEM model utilizes the cohesive crack model to achieve simulation of the fracturing process, however, in this study, we did not observe grain breakage from the experimental results, which is supported by the particle size distribution (PSD) of the grains from the first and last micro-CT scan image data (Figure 5). Thus, the FDEM model we implement considers only the interaction of grains and no grain breakage is simulated.

The digital twin of the tested sample is configured to statistically resemble the laboratory sample, in terms of, grain numbers, grain size distribution, and grain morphological features. Each grain was meshed into many second-order tetrahedral finite elements (Figure 6). In addition, a typical FDEM model involving fracturing requires an iterative calibration process (Tatone & Grasselli, 2015); however, in this study, no calibration was conducted, and the basic material parameters are assigned to the grains (Table 1).

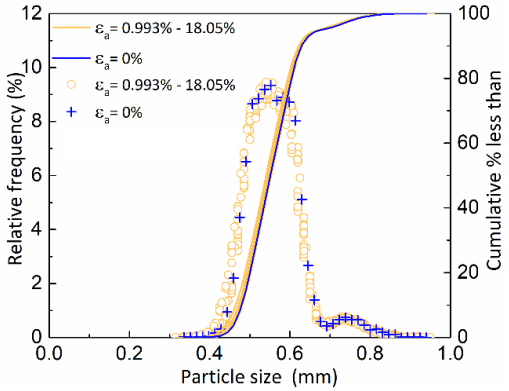

Figure 5: Particle size distribution (PSD) of the laboratory sample at the first and last micro-CT scan data.

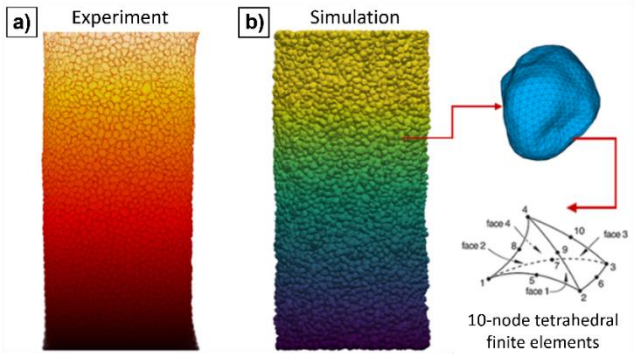

Figure 6: Creation of the digital twin of the laboratory sample.

Table 1: Material parameters used in the FDEM simulation (from Chen et al., 2021).

Parameter (unit)	Value
Density (kg/m^3)	2650
Young's modulus (GPa)	92.1
Poisson's ratio (-)	0.118
Friction coefficient (-)	0.5
Normal and tangential penalty (N/m^3)	92.1×10^{11}
Damping factor (0.03)	0.03

3 Results and Discussion

3.1 Macroscopic Stress-strain Behaviour

The FDEM model, without calibration against the experimental results, reasonably reproduces the macroscopic behaviours of the laboratory sample including the stress-strain and dilation behaviours (Figure 7). The simulation shows an earlier peak stress ratio σ_1/σ_3 than the experiment, which may be related to the micro-CT scans conducted before the peak.

The overall consistency suggests that the critical information needed in the modelling of granular material are particle shape and packing properties, which is confirmed by other researchers (Kawamoto et al., 2018). Note that, the drop in stress ratio during each scan is due to the stress relaxation caused by the loading pause during each X-ray imaging.

We choose six strain intervals (I-VI) for further analyse: 0.00% – 0.99%, 0.99% – 5.03%, 5.03% – 8.06%, 8.06% – 11.06%, 11.06% – 14.06%, and 14.06% – 18.06%, which are divided by five strain states marked A-E in Figure 7.

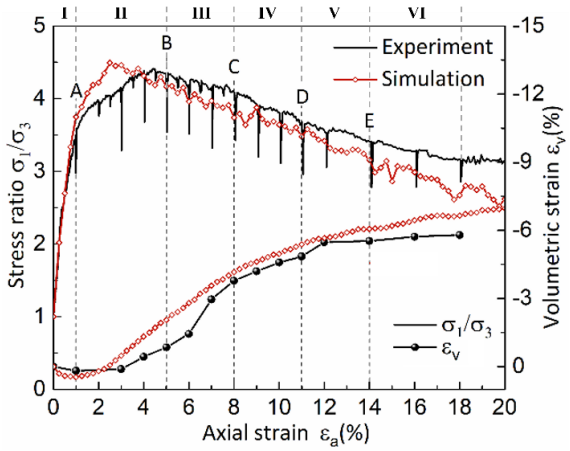

Figure 7: Stress-strain and dilation curves of the experimental and numerical simulated results. Strain point A-E divides the loading process into six incremental strain steps (I-VI) that are further evaluated.

3.2 Microscopic Particle Dynamics

We identified 15961 individual particles in the tested sample. We further compare the incremental particle displacements at six strain states to examine the particle kinematics obtained from the experiment and the FDEM simulation (Figure 8). The FDEM simulated particle displacement field is in good agreement with that obtained in the experiment. The magnitude of particle displacement increases with the shearing process and bulging are shown in all the steps. Two cone-shaped dead zones are developed at the top and bottom of the sample at the post-peak softening stages. While in the middle of the sample, a zone of intensive shearing localizes into an X-shaped shear band.

Proceedings DOI: 10.21467/proceedings.133
ISBN: 978-81-957605-1-0

Series: AIJR Proceedings
ISSN: 2582-3922

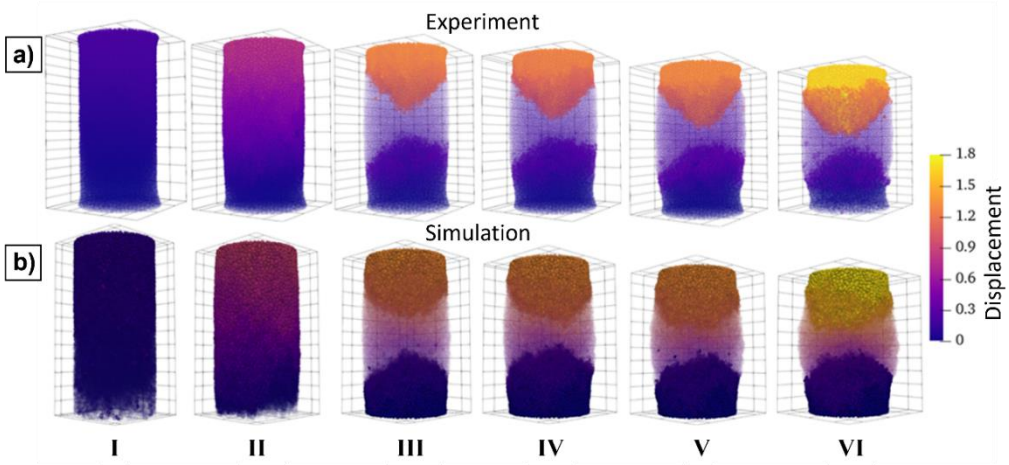

Figure 8: Particle displacements at incremental strain steps for (a) experimental test and (b) FDEM simulation.

At the microscopic scale, the grains rearrange themselves in response to the shear deformation, and the varying local structures of particles creates highly heterogeneous particle motion. As a result, granular materials deform in a nonaffine form (Ma et al, 2018), that is, non-uniform rotation, deformation and rearrangement of particles. The micro-CT image data and FDEM simulation allow us to quantify the nonaffine motion of particle using the local minimum nonaffine displacement $D^2_{\min}$ that measures the mean square deviation of the particle's position from the best-fit affine transformation of its neighbourhood over the strain interval $\delta\varepsilon$ (Falk & Langer, 1998; Ding et al., 2014; Cubuk et al., 2017):

$$D^2_{\min}\left(\varepsilon, \varepsilon+\delta\varepsilon\right) = \frac{1}{N_i}\sum_{k}^{N_i}\left[\boldsymbol{\mu}_{ki}(\varepsilon+\delta\varepsilon) - \boldsymbol{\Lambda}_i(\varepsilon)\boldsymbol{\mu}_{ki}(\varepsilon)\right]^2 \quad \textbf{(6)}$$

where $\boldsymbol{\Lambda}_i(\varepsilon)$ is the best-fit affine deformation tensor of particle i extracted by minimizing the $D^2_{\min}\left(\varepsilon,\varepsilon+\delta\varepsilon\right)$ (Chikkadi & Schall, 2012; Guo & Zhao, 2014):

$$\boldsymbol{\Lambda}_i = \mathbf{X}\cdot\mathbf{Y}^{-1} \quad \textbf{(7)}$$

$$\mathbf{X} = \sum_{k}^{N_i}\boldsymbol{\mu}_{ki}(\varepsilon+\delta\varepsilon)\otimes\boldsymbol{\mu}_{ki}(\varepsilon) \quad \textbf{(8)}$$

$$\mathbf{Y} = \sum_{k}^{N_i}\boldsymbol{\mu}_{ki}(\varepsilon)\otimes\boldsymbol{\mu}_{ki}(\varepsilon) \quad \textbf{(9)}$$

where $\boldsymbol{\mu}_{ki}(\varepsilon)$ is the displacement vector between the reference particle i and its neighbour k at strain state ε. Note that the nonaffinity measure depends on the size of the neighbourhood. Here, we take the first minimum of the pair-correlation function as the cutoff distance (Chikkadi & Schall, 2012; Chen et al., 2021). Our results showed that probability distribution functions of the local minimum nonaffine displacement $D^2_{\min}$ exhibits a power-law decay, which implies that particles with large nonaffine displacements are collectively organized, and particles with similar nonaffine displacements tend to form compact clusters (Kou et al., 2018; Chen et al., 2021).

The local strain tensor is determined based on the affine tensor $\boldsymbol{\Lambda}$ using: $\boldsymbol{\varepsilon}^L = -\left(\boldsymbol{\Lambda}+\boldsymbol{\Lambda}^T\right)/2$, and the local deviatoric strain for each particle can be calculated as $\varepsilon_q^L = \sqrt{\frac{2}{3}\boldsymbol{\varepsilon}^L_{dev}:\boldsymbol{\varepsilon}^L_{dev}}$. The local deviatoric strain ε_q^L are evaluated at strain intervals I-V (Figure 9).

Similar spatial distribution and temporal evolution of the granular system are observed in the experimental and numerical results. At 1.0% axial strain, a few localized plastic zones appeared randomly in the elastically deformed surroundings. After the onset of yielding, particles rearrange themselves to accommodate the increased strain, and many activated plastic zones appeared. These

zones are characterized by close-packed particles with high local strain magnitude. Eventually, those plastic zones coalescence into a conjugate X-shaped shear band spanning the granular system. Once the shear band is formed, the subsequent plastic activity is essentially dominated by the evolution of the shear band through thickening and sliding.

Although the evolution patterns of the granular systems observed in experiment and simulation show great similarities, the thickness and spanning region of the shear band are slightly different. This may be related to the fact that the FDEM simulation lacks the consideration of multiscale contacting behaviour of particles. The FDEM contact model assumes the contact point is fully sticking before reaching the Column frictional resistance. For real particles with multiscale morphological characteristics may experience relative motion even under tiny perturbation and affect the local rearrangement of particles (Kou et al., 2017). In addition, a constant sliding friction coefficient is applied to the FDEM model, which ignores the variable friction conditions in actual particle surfaces.

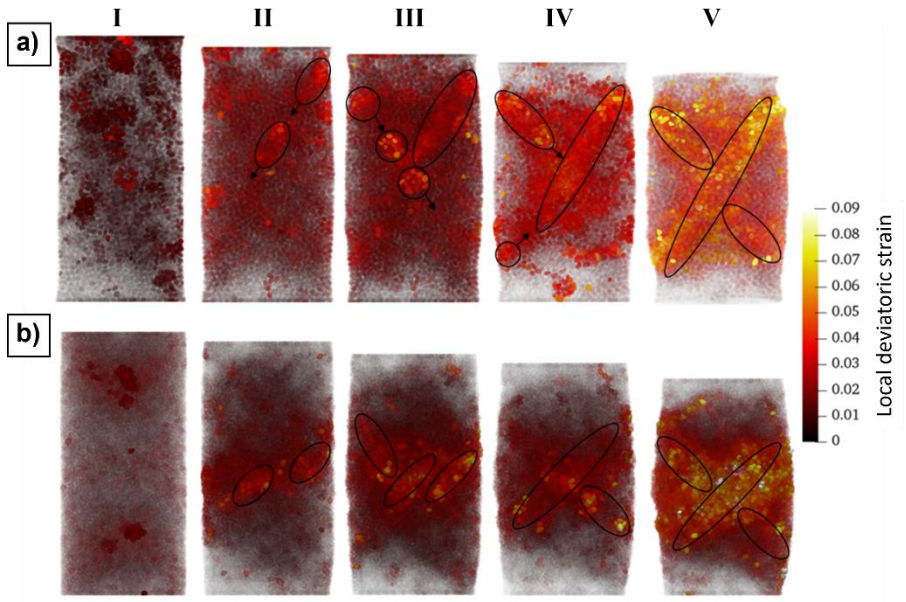

Figure 9: The spatial distribution of local deviatoric strain at strain states I-V for both (a) experiment and (b) numerical simulation. The yellow and red indicate particles subjected to large local deviatoric strain, and particles with small are coloured black and are transparent.

In this study, the grain size is relatively large at the millimetre scale, and with the high-resolution micro-CT scan, almost all the grains were captured with high image quality. In some cases, for example, when clay samples are examined, the grain size may be at the micrometre scale that the micro-CT imaging may not be able to resolve each individual grain. In those cases, segmentation-based image analysis would not be applicable. Instead, a direct estimation of the spatial variation of density can be achieved through a correlation between grayvalues and density.

4 Conclusions

In this work, weinvestigate the mechanical behaviour of granular materials by combining the merits of the in-situ testing under X-ray micro-CT and FDEM numerical modelling. We perform spherical harmonic analysis to characterize and reconstruct the multiscale morphological characteristics of irregularly shaped particles, which enables accurate matching of particles even at the large strain intervals. Relying on the detailed spherical harmonic reconstruction, we establish high fidelity numerical model with the consistent particle morphology and disordered structure. The FDEM simulation results quantitatively agree with the overall response recorded in the experiment test. The particle scale dynamics including the nonaffine particle displacements and particle clustering behaviour show a remarkable quantitative agreement between simulation and experiment. Our results demonstrated that the spatiotemporal evolution of localized microscopic scale plastic deformation controls the macroscopic responses of the granular system. The proposed tool in this study sheds light

Proceedings DOI: 10.21467/proceedings.133
ISBN: 978-81-957605-1-0

Series: AIJR Proceedings
ISSN: 2582-3922

on bridging the microscopic and macroscopic mechanical behaviour of granular materials by 3D visualization and quantitative analysis. This providing us with a better understanding of the physical mechanisms behind the failure of granular systems, such as failure of soil slopes and weakening of gouge filled fault zones.

5. Declarations

5.1 Acknowledgements

Q. Zhao is supported by the FCE Start-up Fund for New Recruits at PolyU (Project ID P0034042) and the Early Career Scheme of the Research Grants Council of the Hong Kong Special Administrative Region, China (Project No. PolyU 25220021).

5.2 Publisher's Note

AIJR remains neutral with regard to jurisdictional claims in published maps and institutional affiliations.

References

Afshar, T., Disfani, M. M., Narsilio, G. A., & Arulrajah, A. (2018). Post-breakage changes in particle properties using synchrotron tomography. Powder Technology, 325, 530-544.

Alshibli, K. A., Jarrar, M. F., Druckrey, A. M., & Al-Raoush, R. I. (2016). Influence of particle morphology on 3D kinematic behavior and strain localization of sheared sand. Journal of Geotechnical and Geoenvironmental Engineering, 143(2), 04016097.

Andrade, J. E., & Avila, C. F. (2012). Granular element method (GEM): linking inter-particle forces with macroscopic loading. Granular Matter, 14(1), 51-61.

Andò, E., Hall, S. A., Viggiani, G., Desrues, J., & Bésuelle, P. (2012). Grain-scale experimental investigation of localised deformation in sand: a discrete particle tracking approach. Acta Geotechnica, 7(1), 1-13.

Chen, Y., Ma, G., Zhou, W., Wei, D., Zhao, Q., Zou, Y., & Grasselli, G. (2021). An enhanced tool for probing the microscopic behavior of granular materials based on X-ray micro-CT and FDEM. Computers and Geotechnics, 132, 103974.

Cheng, Z., & Wang, J. (2018). Experimental investigation of inter-particle contact evolution of sheared granular materials using X-ray micro-tomography. Soils and Foundations, 58(6), 1492-1510.

Chevalier, B., Tsutsumi, Y., & Otani, J. (2019). Direct shear behavior of a mixture of sand and tire chips using X-ray computed tomography and discrete element method. International Journal of Geosynthetics and Ground Engineering, 5(2), 7.

Chikkadi, V., & Schall, P. (2012). Nonaffine measures of particle displacements in sheared colloidal glasses. Physical Review E, 85(3), 031402.

Cubuk, E.D., Ivancic, R.J.S., Schoenholz, S.S., Strickland, D.J., Basu, A., Davidson, Z.S., Fontaine, J., Hor, J.L., Huang, Y.R., Jiang, Y. and Keim, N.C. (2017). Structure-property relationships from universal signatures of plasticity in disordered solids. Science, 358(6366), 1033-1037.

Ding, J., Patinet, S., Falk, M. L., Cheng, Y., & Ma, E. (2014). Soft spots and their structural signature in a metallic glass. Proceedings of the National Academy of Sciences, 111(39), 14052-14056.

Falk, M. L., & Langer, J. S. (1998). Dynamics of viscoplastic deformation in amorphous solids. Physical Review E, 57(6), 7192.

Garboczi, E. J. (2002). Three-dimensional mathematical analysis of particle shape using X-ray tomography and spherical harmonics: Application to aggregates used in concrete. Cement and concrete research, 32(10), 1621-1638.

Guo, N., & Zhao, J. (2014). Local fluctuations and spatial correlations in granular flows under constant-volume quasistatic shear. Physical Review E, 89(4), 042208.

Karatza, Z., Andò, E., Papanicolopulos, S. A., Ooi, J. Y., & Viggiani, G. (2017). Evolution of deformation and breakage in sand studied using X-ray tomography. Géotechnique, 68(2), 107-117.

Kong, D., & Fonseca, J. (2019). On the kinematics of shelly carbonate sand using X-ray micro tomography. Engineering Geology, 261, 105268.

Kawamoto, R., Andò, E., Viggiani, G., & Andrade, J. E. (2016). Level set discrete element method for three-dimensional computations with triaxial case study. Journal of the Mechanics and Physics of Solids, 91, 1-13.

Kawamoto, R., Andò, E., Viggiani, G., & Andrade, J. E. (2018). All you need is shape: Predicting shear banding in sand with LS-DEM. Journal of the Mechanics and Physics of Solids, 111, 375-392.

Kazhdan, M., Funkhouser, T., & Rusinkiewicz, S. (2003, June). Rotation invariant spherical harmonic representation of 3 d shape descriptors. In Symposium on geometry processing (Vol. 6, pp. 156-164).

Kou, B., Cao, Y., Li, J., Xia, C., Li, Z., Dong, H., Zhang, A., Zhang, J., Kob, W. & Wang, Y. (2017). Granular materials flow like complex fluids. Nature, 551(7680), 360-363.

Kou, B., Cao, Y., Li, J., Xia, C., Li, Z., Dong, H., Zhang, A., Zhang, J., Kob, W. and Wang, Y. (2018). Translational and rotational dynamical heterogeneities in granular systems. Physical review letters, 121(1), 018002.

Murphy, K. A., Dahmen, K. A., & Jaeger, H. M. (2019). Transforming Mesoscale Granular Plasticity Through Particle Shape. Physical Review X, 9(1), 011014.

Ma, G., Zhou, W., & Chang, X. L. (2014). Modeling the particle breakage of rockfill materials with the cohesive crack model. Computers and Geotechnics, 61, 1320–1143.

Ma, G., Zhou, W., Chang, X.-L., & Chen, M.-X. (2016). A hybrid approach for modeling of breakable granular materials using combined finite-discrete element method. Granular Matter, 18(1), 7.

Ma, G., Regueiro, R. A., Zhou, W., Wang, Q., & Liu, J. (2018). Role of particle crushing on particle kinematics and shear banding in granular materials. Acta Geotechnica, 13(3), 601–618.

Majmudar, T. S., & Behringer, R. P. (2005). Contact force measurements and stress-induced anisotropy in granular materials. Nature, 435(7045), 1079.

Saadatfar, M., Sheppard, A. P., Senden, T. J., & Kabla, A. J. (2012). Mapping forces in a 3D elastic assembly of grains. Journal of the Mechanics and Physics of Solids, 60(1), 55-66.

Tatone, B. S., & Grasselli, G. (2015). A calibration procedure for two-dimensional laboratory-scale hybrid finite–discrete element simulations. International Journal of Rock Mechanics and Mining Sciences, 75, 56-72.

Wei, D., Wang, J., & Zhao, B. (2018). A simple method for particle shape generation with spherical harmonics. Powder technology, 330, 284-291.

Weis, S., & Schröter, M. (2017). Analyzing X-ray tomographies of granular packings. Review of Scientific Instruments, 88(5), 051809.

Wu, M., Wang, J., Russell, A., & Cheng, Z. (2020). DEM modelling of mini-triaxial test based on one-to-one mapping of sand particles. Géotechnique, 1-14.

Zhao, B. D., Wei, D. H., & Wang, J. F. (2017). Particle shape quantification using rotation-invariant spherical harmonic analysis. Géotechnique Letters, 7(2), 190-196.

Zhou, B., Wang, J., & Wang, H. (2018). A novel particle tracking method for granular sands based on spherical harmonic rotational invariants. Géotechnique, 68(12), 1116-1123.

Zhao, Q., Tisato, N., & Grasselli, G. (2017). Rotary shear experiments under X-ray micro-computed tomography. Review of Scientific Instruments, 88(1), 015110.

Zhao, Q., Tisato, N., Kovaleva, O., & Grasselli, G. (2018). Direct Observation of Faulting by Means of Rotary Shear Tests Under X-Ray Micro-Computed Tomography. Journal of Geophysical Research: Solid Earth, 123(9), 7389-7403.

Zhao, Q., Glaser, S. D., Tisato, N., & Grasselli, G. (2020). Assessing energy budget of laboratory fault slip using rotary shear experiments and micro-computed tomography. Geophysical Research Letters, 47(1), e2019GL084787.

Zhou, B., Wang, J., & Zhao, B. (2015). Micromorphology characterization and reconstruction of sand particles using micro-X-ray tomography and spherical harmonics. Engineering geology, 184, 126-137.

Proceedings DOI: 10.21467/proceedings.133
ISBN: 978-81-957605-1-0

Series: AIJR Proceedings
ISSN: 2582-3922